SANDIA NATIONAL LABORATORIES
WASTE ISOLATION PILOT PLANT

ANALYSIS REPORT FOR MODELING THE CASTILE PRESSURIZED BRINE RESERVOIR
REVISION 0

Author:	Paul Docherty	Paul Docherty	5/2/2023
	Print	Signature	Date
Technical Reviewer:	Cliff Hansen	*Signature on file*	5/2/2023
	Print	Signature	Date
Technical Reviewer:	Seth King		5/2/2023
	Print	Signature	Date
QA Reviewer:	Jennifer Long	Jennifer Long	5/2/23
	Print	Signature	Date
Management Reviewer:	Steve Wagner		5/2/2023
	Print	Signature	Date

ERMS #~~578975~~ 578976 gd 5/2/23

APRIL 2023

WIPP:4.4.1.1.1:PA:QA-L:578975

Information Only

This page intentionally left blank.

Information Only

TABLE OF CONTENTS

EXECUTIVE SUMMARY 5

1.0 INTRODUCTION 6

2.0 BRIEF OVERVIEW OF THE CASTILE BRINE RESERVOIR 7

3.0 CASTILE BRINE RESERVOIR MODELS 9

3.1 Model CRA19 9

3.2 Model CBV 11

3.3 Model CBX4 11

3.4 Summary 12

4.0 RESULTS 13

5.0 ANALYSIS OF RESULTS 16

5.1 Brine reservoir pressure: CBV vs CRA19 19

5.2 Brine reservoir pressure: CBX4 vs CRA19 19

6.0 SENSITIVITY ANALYSIS 20

7.0 IMPLEMENTATION 24

7.1 Model CBV 24

7.2 Model CBX4 24

7.3 Execution on Linux cluster 25

8.0 SUMMARY AND RECOMMENDATION 25

9.0 REFERENCES 26

APPENDIX A: MEAN VALUES IN TABLE 1 27

Information Only

LIST OF TABLES

Table 1: Summary of Castile brine reservoir parameters 13
Table 2: Stepwise ranked regression for brine flow up the borehole 23
Table 3: Stepwise ranked regression for waste pressure 23
Table 4: Stepwise ranked regression for waste brine saturation 23

LIST OF FIGURES

Figure 1: Grid Model CRA19 (the CRA-2019 PA BRAGFLO grid model) 10
Figure 2: Grid Model CBX4 12
Figure 3: Total releases 14
Figure 4: Direct brine releases 14
Figure 5: Releases from the Culebra 15
Figure 6: Spallings releases 15
Figure 7: Cuttings and cavings releases 16
Figure 8: Brine flow up the borehole 17
Figure 9: Pressure in the Castile brine reservoir 18
Figure 10: Waste pressure 18
Figure 11: Waste brine saturation 19
Figure 12: Comparison of brine flow (top), waste pressure (middle), and waste saturation (bottom), for Models CRA19, CBV and CBX4 (Replicate 1, Scenario 3) 22
Figure 13: Triangular probability distribution 27

Information Only

Executive Summary

Parameters describing the Castile brine reservoir have been the subject of some uncertainty in WIPP Performance Assessment. Descriptions of the reservoir's connectivity, porosity, and compressibility have all evolved with time as understanding has improved. A recent report by Gross and Gjerapic (2022) addresses one further aspect of the brine reservoir, namely its maximum volume. The authors use historical pressure data from two wells, WIPP-12 and ERDA-6, along with methodology well-established in petroleum engineering, to produce new estimates of the Castile reservoir's maximum volume. This report assesses the impact of revising the Castile reservoir maximum volume to the maximum volume obtained by Gross and Gjerapic using well data from WIPP-12. At 5.9×10^6 m^3, Gross and Gjerapic's estimate is about one third the value currently being used in WIPP performance assessment (PA) calculations.

The analysis considers both the maximum reservoir volume and the representation of the reservoir volume in the computational grid. Of particular interest are the values of reservoir porosity in the PA model; currently, these are not representative of actual porosities in the Castile anhydrite. It is demonstrated that by incorporating Gross and Gjerapic's volume estimate into the PA model and, in addition, by expanding the reservoir in the PA computational grid, model reservoir porosity can be brought in line with historical Castile porosity estimates. The revised porosity values may then be used to set reservoir pore compressibility consistent with the way it is set for other materials in PA.

It is recommended that Gross and Gjerapic's maximum volume estimate be adopted and that its implementation in PA be carried out by widening the Castile brine reservoir beyond the edges of the repository in the computational grid. Maximum reservoir volume is then consistent with pressure tests at nearby well WIPP-12, porosity in the Castile reservoir can be set within a physically realistic range, and treatment of pore compressibility in the reservoir can be improved. All combined, these changes produce only a small reduction in modeled releases from the repository compared to CRA-2019 levels.

Information Only

1.0 INTRODUCTION

The Waste Isolation Pilot Plant (WIPP), located in southeastern New Mexico, has been developed by the U.S. Department of Energy (DOE) for the geologic (deep underground) disposal of transuranic (TRU) waste. Containment of TRU waste at the WIPP is regulated by the U.S. Environmental Protection Agency (EPA) according to the regulations set forth in Title 40 of the Code of Federal Regulations (CFR), Part 191.

The DOE demonstrates compliance with the containment requirements according to the Certification Criteria in Title 40 CFR Part 194 by means of performance assessment (PA) calculations performed by Sandia National Laboratories. WIPP PA calculations estimate the probability and consequence of potential radionuclide releases from the repository to the accessible environment for a regulatory period of 10,000 years after facility closure.

The models used in PA are maintained and updated with new information as part of an ongoing process. Improved information regarding important WIPP features, events, and processes (FEPs) typically results in refinements and modifications to PA models and the parameters used in them. Planned changes to the repository and/or the components therein also result in updates to WIPP PA models. WIPP PA models are used to support the repository recertification process that occurs at five-year intervals following the receipt of the first waste shipment at the site in 1999.

This Analysis Report follows up Analysis Plan 196 (King et al., 2022) and concerns a hypothetical pressurized brine reservoir that may lie within the Castile anhydrite formation directly beneath the WIPP repository. In a recent report prepared for the Nuclear Waste Partnership, Gross and Gjerapic (2022) used historical test data from two wells in the vicinity of the repository to estimate the volume of brine in the Castile reservoir. The wells were WIPP-12 and ERDA-6; both wells encountered pressurized brine in the Castile. Data from the WIPP-12 well have been used to establish a model for a reservoir that may underlie the WIPP repository (U.S. Environmental Protection Agency, 1997). Data include long-term pressure measurements useful for bounding the reservoir's size. Gross and Gjerapic used a radially symmetric reservoir model with different near- and far-field properties, which they adjusted to match both short- and long-term pressure response. While the brine reservoir volume has been estimated before (Popielak et al., 1983; Beauheim, 1996), the results obtained by Gross and Gjerapic are believed to be more accurate. For the ERDA-6 data, Gross and Gjerapic obtained an upper bound on the reservoir volume between 2.3×10^5 and 3.6×10^5 m^3. For WIPP-12 the upper bound was estimated to lie between 3.1×10^6 and 5.9×10^6 m^3. The larger of these WIPP-12 estimates is about one third the maximum reservoir volume currently in use in PA models. Gross and Gjerapic consider the WIPP-12 data to be most relevant to a potential brine reservoir beneath the repository, as does the EPA (U.S. Environmental Protection Agency, 1998).

This report adopts 5.9×10^6 m^3 as the maximum Castile reservoir volume and considers two options for implementing it: (i) a PA model in which the reservoir porosity is simply reduced by about one third from its current range of values; and (ii) a PA model in which porosity is reduced and, in addition, the reservoir is extended laterally in the modeling grid. Both options are designed to realize the new maximum reservoir volume; however, the second option seeks to achieve it with a physically realistic range of porosity and is the option favored here.

Information Only

The report begins with a brief overview of the Castile brine reservoir, specifically the relationships between bulk compressibility, porosity, and brine reservoir volume. PA's treatment of pore compressibility in the reservoir is also discussed. Three models are then introduced: the current PA model and two models that implement Gross and Gjerapic's maximum reservoir volume. PA results for the three models are presented and analyzed; here the focus is on reservoir productivity, how it is different in the three models, and how it affects pressure and brine saturation in the repository. A sensitivity analysis then looks at uncertainty in outcomes and whether parameters that most influence uncertainty are the same, or different, for the three models. The report concludes with some implementation details, a brief summary, and a recommendation for a new representation of the Castile brine reservoir in upcoming PAs.

2.0 BRIEF OVERVIEW OF THE CASTILE BRINE RESERVOIR

Three parameters describe the material properties of the Castile brine reservoir in PA: (i) initial pressure (CASTILER:PRESSURE); (ii) permeability (CASTILER:PRMX_LOG); and (iii) bulk compressibility (CASTILER:COMP_RCK). This brief overview concerns only the bulk compressibility, designated below as c_b, and the quantities PA derives from it.

In his 1996 memo, Beauheim proposed the following range of values for c_b:

$$2.0 \times 10^{-11} \leq c_b \leq 1.0 \times 10^{-10} \quad [\mathrm{Pa}^{-1}] \ . \tag{1}$$

To arrive at Eq. 1, Beauheim started with a bulk compressibility value of 1.0×10^{-11} [Pa^{-1}] derived from acoustic log data and adjusted it by a factor ranging from 2 to 10 to take into account fracturing in the Castile anhydrite (see also Popielak et al., 1983). In the same memo, Beauheim went further and estimated a range for the volume of brine in the Castile, that is, a range for the Castile reservoir pore volume V_ϕ. To within round off, his range is

$$3.4 \times 10^{6} \leq V_\phi \leq 1.7 \times 10^{7} \quad [\mathrm{m}^3] \ . \tag{2}$$

To obtain Eq. 2, Beauheim used depletion data from well WIPP-12, reported by Popielak et al. (1983), and the formula describing pore compressibility c_ϕ:

$$\frac{dV_\phi}{dP} = c_\phi V_\phi \approx \frac{c_b}{\phi} V_\phi \ . \tag{3}$$

Here, P is pore pressure and ϕ is the porosity of the brine reservoir. (In all equations below, ϕ is specifically the initial porosity in the brine reservoir.) The approximation in Eq. 3 is valid if the compressibility of the intrinsic rock material is small in comparison to the bulk compressibility. The quantity dV_ϕ/dP in Eq. 3 is known as the Productivity Ratio, or PR. PR measures reservoir productivity as the quotient of the volume produced from the reservoir and the corresponding drop

Information Only

in reservoir pore pressure[1]. The WIPP-12 depletion data yield a value of 0.04 for PR. For porosity, Beauheim used the constant from the CCA: $\phi = 0.0087$. These values in Eq. 3, along with bulk compressibility from Eq. 1, give the range in Eq. 2.

Both the range in Eq. 1 for bulk compressibility and the range in Eq. 2 for pore volume were adopted by the EPA and have been used in PA since 2004. Bulk compressibility is a sampled parameter in PA described by a triangular distribution with minimum and maximum values given by Eq. 1, a mode equal to 4.0×10^{-11} [Pa^{-1}], and a mean value of 5.33×10^{-11} [Pa^{-1}]. Reservoir volume, on the other hand, is not a sampled parameter. To understand how the range in Eq. 2 is implemented in PA, first write the relationship between reservoir pore volume and the volume V of the PA model grid cells assigned to describe the brine reservoir:

$$V_\phi = \phi V \quad . \tag{4}$$

Next, note that PA uses a linear mapping from bulk compressibility to initial porosity in the Castile brine, as described by Stein (2003):

$$\phi = \frac{c_b}{\alpha} \quad , \tag{5}$$

where α is a positive constant. Clearly, α is closely related to pore compressibility. A consequence of Eq. 5 is that porosity follows a triangular distribution geometrically similar to that of bulk compressibility (Stein, 2003). Since V is constant, the same is also true of V_ϕ. The constant α is chosen so that maximum porosity (realized at maximum bulk compressibility) yields the desired maximum reservoir pore volume. The same value of α gives a minimum porosity (at minimum bulk compressibility) that produces the desired minimum reservoir pore volume. (To understand why, see Eq. 8 below.) The relevant relationships for determining α are

$$\alpha = \frac{c_b^{min}}{\phi^{min}} = \frac{c_b^{max}}{\phi^{max}} \quad \text{and} \quad \phi^{min} = \frac{V_\phi^{min}}{V} \;,\; \phi^{max} = \frac{V_\phi^{max}}{V} \quad , \tag{6}$$

where superscripts denote minimum and maximum values. In the CRA-2004 model, the Castile reservoir grid cells have a volume 1.846×10^{7} m^3, the corresponding value of α is 1.0860×10^{-10}, and the range of porosity is

$$0.1842 \leq \phi \leq 0.9208 \quad . \tag{7}$$

[1] In CRA-2019, Productivity Ratio is defined as PR = $\frac{c_b}{\phi}V$, where V is grid volume (US DOE, 2019, Appendix PA-2019). CRA-2019's PR is not a measure of $\frac{dV_\phi}{dP}$.

Information Only

As the EPA points out (U.S. Environmental Protection Agency, 1997, Appendix PD, page PD-12), the porosities in Eq. 7 are not physically realistic, but they are necessary if the desired brine reservoir volumes are to be achieved within the CRA-2004 grid cell volume mentioned above.

A consequence of the PA approach is that the following ratios are equal:

$$\frac{c_b^{max}}{c_b^{min}} = \frac{V_\phi^{max}}{V_\phi^{min}} = \frac{\phi^{max}}{\phi^{min}} \quad . \tag{8}$$

The first equality here results from Beauheim's method for estimating the reservoir pore volume; recall, he used a fixed porosity to produce his estimate. While PA continues to use Beauheim's range of reservoir pore volume, it implements a variable porosity directly related to bulk compressibility to achieve it, as described above; this leads to the second equality in Eq. 8. Since only bulk compressibility is a sampled parameter, it determines the value of the ratios in Eq. 8. This means, for example, that if V_ϕ^{max} were to change (via a change to an input file specifying the value of α), then V_ϕ^{min} would automatically adjust to maintain the ratio set by the bulk compressibility.

Finally, it was mentioned above that the constant α is closely related to pore compressibility. This may suggest that PA is using a constant reservoir pore compressibility in its flow computations; however, this is not currently the case. Perhaps because of the large initial porosities (Eq. 7), PA sets its reservoir pore compressibility variable POR_COMP to c_b/0.0087, that is, it sets pore compressibility equal to bulk compressibility divided by a *physically reasonable* porosity value, namely the one used in the CCA. In this way, large PA initial porosities do not contaminate the magnitude of reservoir pore compressibility used in flow computations.

To summarize, the PA approach described above maps bulk compressibility to an artificially large range of initial porosity values in order to realize a desired range of brine reservoir volumes within a fixed set of cells in the modeling grid; PA sets reservoir pore compressibility using a variable bulk compressibility and a physically reasonable, but constant, value of porosity.

3.0 CASTILE BRINE RESERVOIR MODELS

Three different models of the Castile brine reservoir are described in this section. The first, named CRA19, is from the CRA-2019 PA. The second, called CBV, uses the same grid as CRA19, but reduces porosity in the Castile brine reservoir in order to achieve the maximum reservoir volume determined by Gross and Gjerapic (2022) from the WIPP-12 data. The third model, called CBX4, uses Gross and Gjerapic's maximum reservoir volume, but expands the reservoir laterally by assigning to it more grid cells, the result of which is to bring about a more realistic range of porosity. All three models use the range in Eq. 1 for bulk compressibility.

3.1 Model CRA19

The BRAGFLO grid model from the CRA-2019 PA is named simply Model CRA19 here. Model CRA19 is shown below in Figure 1, which is Figure PA-12 in Appendix PA-2019 (US DOE,

Information Only

2019). The grid cells assigned to the Castile brine reservoir have x-axis indices 23-45 in the figure (and y-axis index 1). The brine reservoir has the same lateral extent as the repository.

In CRA-2019 the volume V of the Castile brine grid cells increased compared to its CRA-2004 value[2]. For CRA-2019, $V = 2.178\times10^7$ m^3, which is about 18% greater than the CRA-2004 value mentioned in Section 2 above. The constant α, however, was not updated from its 2004 value for the CRA-2019 PA. As a result, the CRA-2019 range of porosities remained the same as in CRA-2004, while the larger grid volume increased the reservoir volume.

Repeating Eq. 7, Model CRA19's range of porosity is

$$0.1842 \leq \phi \leq 0.9208 \quad , \tag{9}$$

while grid volume V in Eq. 4 gives the range of brine reservoir volume in Model CRA19:

$$4.0 \times 10^6 \leq V_\phi \leq 2.0 \times 10^7 \quad [\mathrm{m}^3] \quad . \tag{10}$$

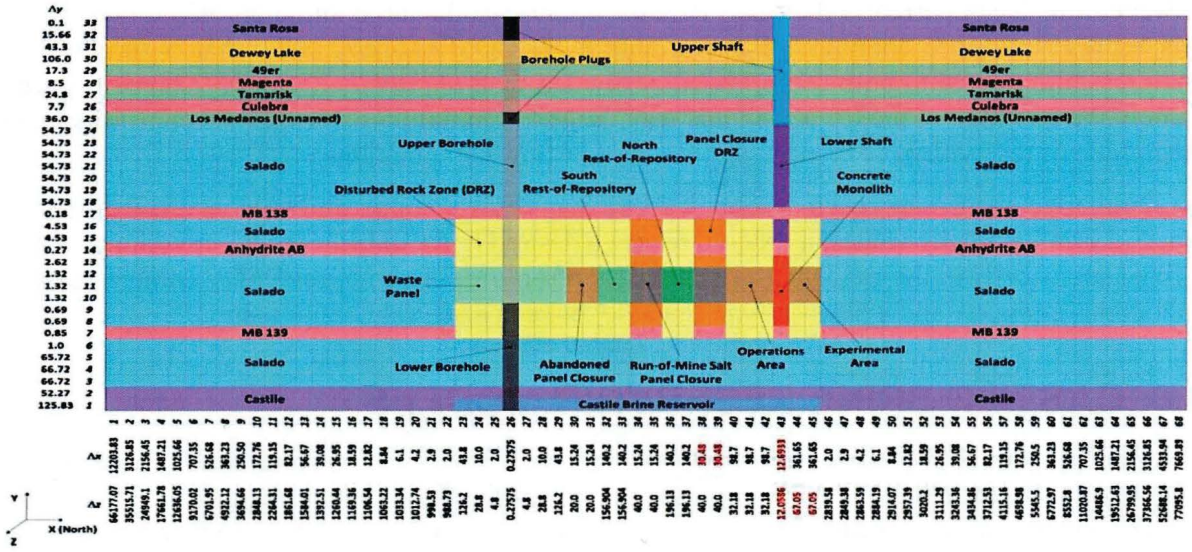


Figure 1: Grid Model CRA19 (the CRA-2019 PA BRAGFLO grid model)

[2] In large part due to increases in both 2014 and 2019 to the Δz values of cells at the north end of the repository (cells with x-indices 44 and 45 in Figure 1).

Information Only

3.2 Model CBV

Model CBV uses the same grid as CRA19 (Figure 1), but reduces porosity to the range

$$0.0542 \leq \phi \leq 0.2709 \quad . \tag{11}$$

The new range is implemented by setting the value of α in Eq. 5 to 3.6915×10^{-10}. Besides this change to α, Model CBV is identical to Model CRA19. The change in porosity brings about a new range of brine reservoir volume:

$$1.18 \times 10^6 \leq V_\phi \leq 5.9 \times 10^6 \ [\mathrm{m}^3] \quad . \tag{12}$$

The value 5.9×10^6 m^3 here is Gross and Gjerapic's (2022) upper bound for the volume of the Castile brine reservoir. Gross and Gjerapic did not estimate a minimum reservoir volume: the minimum volume in Eq. 12 comes from Eq. 8.

3.3 Model CBX4

Model CBX4 assigns grid cells with x-axis indices 9-59 to the Castile brine reservoir, so that the reservoir extends laterally 802.7 m beyond the edges of the repository. Figure 2 shows the extended reservoir in the BRAGFLO grid model. For CBX4, grid volume $V = 7.32\times10^8$, which is about 34 times greater than in Models CRA19 and CBV. The larger grid volume means that Gross and Gjerapic's maximum reservoir volume can be achieved with correspondingly smaller values of porosity. By setting α equal to 1.2407×10^{-8}, the CBX4 range of porosity is

$$0.0016 \leq \phi \leq 0.0081 \quad , \tag{13}$$

while the CBX4 brine reservoir volume range stays the same as in Model CBV:

$$1.18 \times 10^6 \leq V_\phi \leq 5.9 \times 10^6 \ [\mathrm{m}^3] \quad . \tag{14}$$

The range in Eq. 13 is consistent with Popielak et al. (1983), where fracturing in the Castile anhydrite was estimated to bring about effective porosities between 0.001 and 0.01. The upper bound in Eq. 13 is also only slightly less than the value 0.0087 used for porosity in the CCA.

Information Only

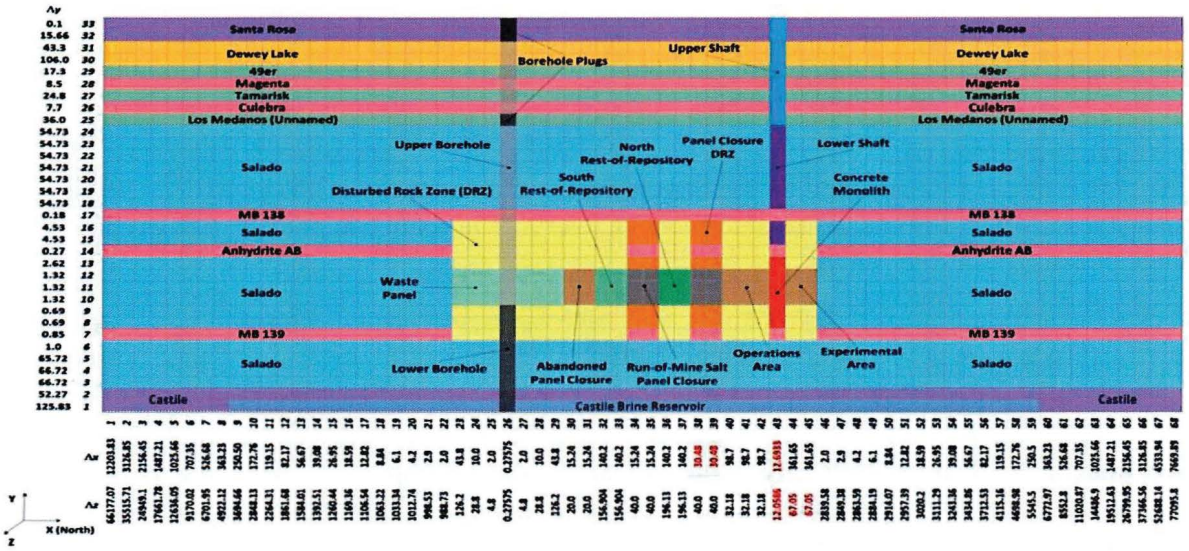


Figure 2: Grid Model CBX4

Lastly, it was mentioned in Section 2 that PA sets its pore compressibility variable POR_COMP to $c_b/0.0087$ in the Castile brine reservoir; this is also the case for Models CRA19 and CBV above. In Model CBX4, on the other hand, POR_COMP in the Castile reservoir is set to c_b/ϕ, consistent with the way it is set for other materials in PA. Note from Eq. 5 that this means the CBX4 Castile reservoir pore compressibility is constant: its value is 1.2407×10^{-8}, the same as the CBX4 value of α. Note further that because the largest porosity in Eq. 13 is less than 0.0087, the reservoir pore compressibility will always be greater in Model CBX4 than in either Model CRA19 or Model CBV.

3.4 Summary

Table 1 summarizes the parameters described above for Models CRA19, CBV and CBX4. In addition, the final column gives the range of Productivity Ratio, PR, for each model. For Models CRA19 and CBV, minimum PR is determined as minimum pore compressibility times minimum reservoir volume; likewise, maximum PR is determined as maximum pore compressibility times maximum pore volume. Since Model CBX4 has constant pore compressibility, the PR range is just that constant times the range of pore volume. Mean values are shown in parentheses for all quantities not constant. Formulas used to derive the mean values are given in Appendix A. Note that the mean PR for Model CBX4 is 0.04. As mentioned in Section 2, 0.04 is the PR obtained from WIPP-12 depletion data reported by Popielak et al. (1983).

Information Only

Table 1: Summary of Castile brine reservoir parameters

Model	Grid vol. V [m^3]	Bulk comp. c_b [Pa^{-1}]	α [Pa^{-1}]	Porosity ϕ	Pore comp. c_ϕ [Pa^{-1}]	Pore vol. V_ϕ [m^3]	PR=$c_\phi V_\phi$ [$m^3\ Pa^{-1}$]
CRA19	2.178×10^{7}	2×10^{-11} - 1×10^{-10} (5.33×10^{-11})	1.0860×10^{-10}	0.1842 - 0.9208 (0.4911)	$c_\phi = \frac{c_b}{0.0087}$ 2.30×10^{-9} - 1.15×10^{-8} (6.13×10^{-9})	4.0×10^{6} - 2.0×10^{7} (1.070×10^{7})	0.009 - 0.23 (0.07)
CBV	2.178×10^{7}	2×10^{-11} - 1×10^{-10} (5.33×10^{-11})	3.6915×10^{-10}	0.0542 - 0.2709 (0.1445)	$c_\phi = \frac{c_b}{0.0087}$ 2.30×10^{-9} - 1.15×10^{-8} (6.13×10^{-9})	1.18×10^{6} - 5.9×10^{6} (3.15×10^{6})	0.003 - 0.07 (0.02)
CBX4	7.32×10^{8}	2×10^{-11} - 1×10^{-10} (5.33×10^{-11})	1.2407×10^{-8}	0.0016 - 0.0081 (0.0043)	$c_\phi = \frac{c_b}{\phi} = const.$ 1.24×10^{-8}	1.18×10^{6} - 5.9×10^{6} (3.15×10^{6})	0.015 - 0.073 (0.04)

4.0 RESULTS

PA results for Models CBV and CBX4 were generated for this report[3]. PA was run for one replicate only, namely Replicate 1, for each model. For Model CRA19, Replicate 1 results were obtained from the CRA-2019 PA. The figures in this section combine results for the three models. The figures show mean value curves obtained by averaging over the 100 parameter vectors in Replicate 1. A single point (p, R) on a curve gives the mean probability p that cumulative release R will be exceeded in the corresponding model.

Figure 3 shows total releases for the three models. Here, Model CBV has the lowest probability at all release amounts, while curves for CBX4 and CRA19 are similar, with CBX4 probabilities slightly less than those for CRA19. Figures 4-7 show the individual components that make up the total releases in Figure 3: direct brine (Figure 4); releases from the Culebra (Figure 5); spallings (Figure 6); and cuttings and cavings (Figure 7). In the case of cuttings and cavings, releases for the three models are identical, and the CBX4 curve overlays those for CRA19 and CBV.

As is typical in WIPP PA, total releases in the three models are dominated by cuttings and cavings at high probabilities, and by direct brine releases at low probabilities. Cuttings and cavings are the solid waste brought to the surface as a result of a drilling intrusion. As described, for example, by Helton (1998, Section 4.5), cuttings and cavings releases are assumed to be independent of repository conditions at the time the intrusion occurs (hence Figure 7). Direct brine releases, on the other hand, do depend on repository conditions. Two main drivers of direct brine releases are pressure and saturation in the waste; how these are affected by conditions in the Castile brine reservoir is taken up in the next section.

[3] Analyses CBV and CBX4 have been archived in CVS. The location of the archive is /data/cvs/CVSLIB/WIPP_EXTERNAL/AP196.

Information Only

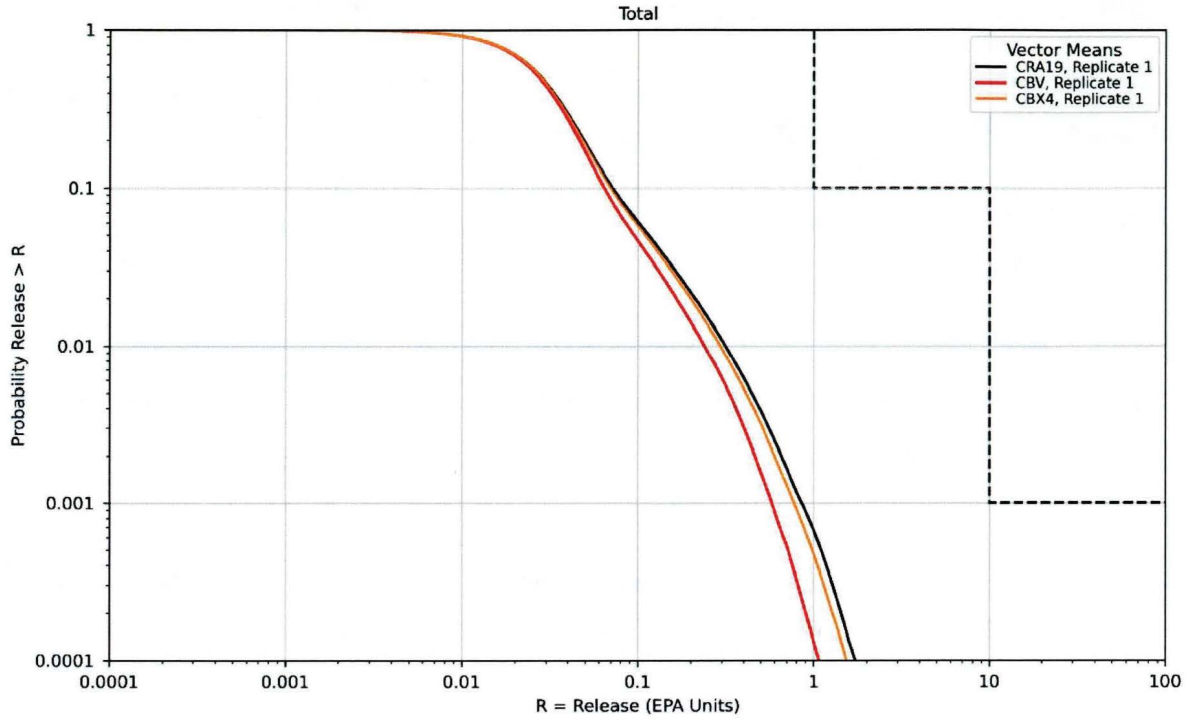


Figure 3: Total releases

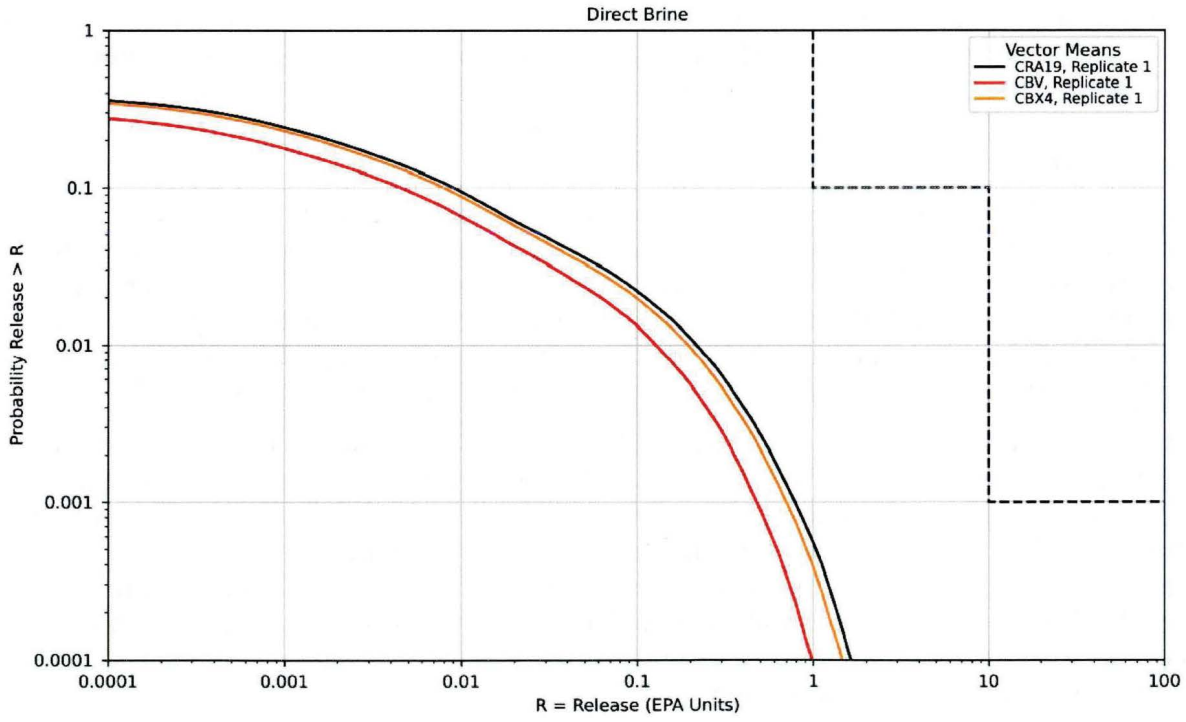


Figure 4: Direct brine releases

Information Only

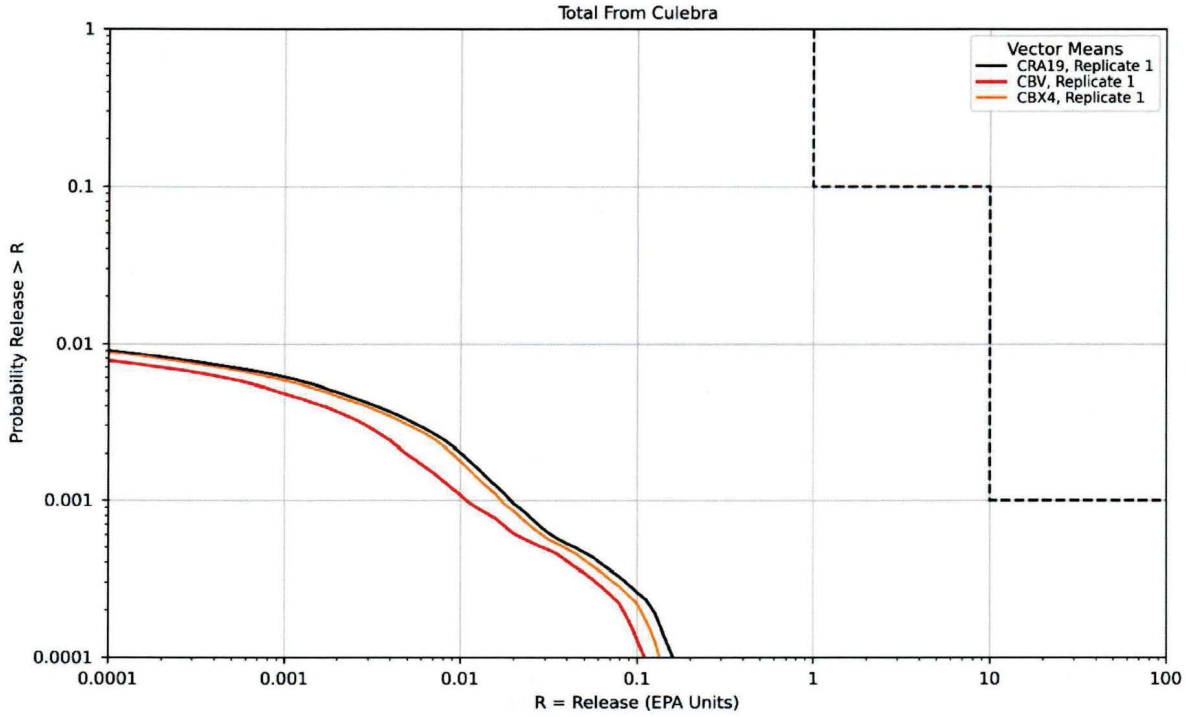


Figure 5: Releases from the Culebra

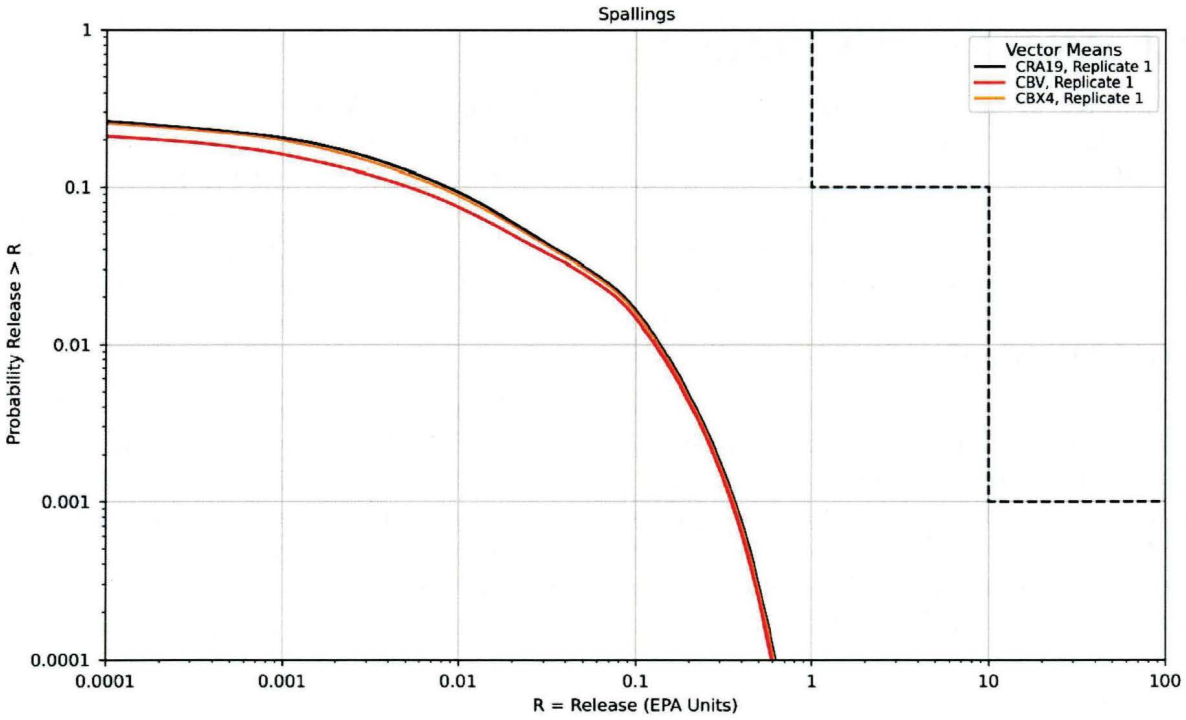


Figure 6: Spallings releases

Information Only

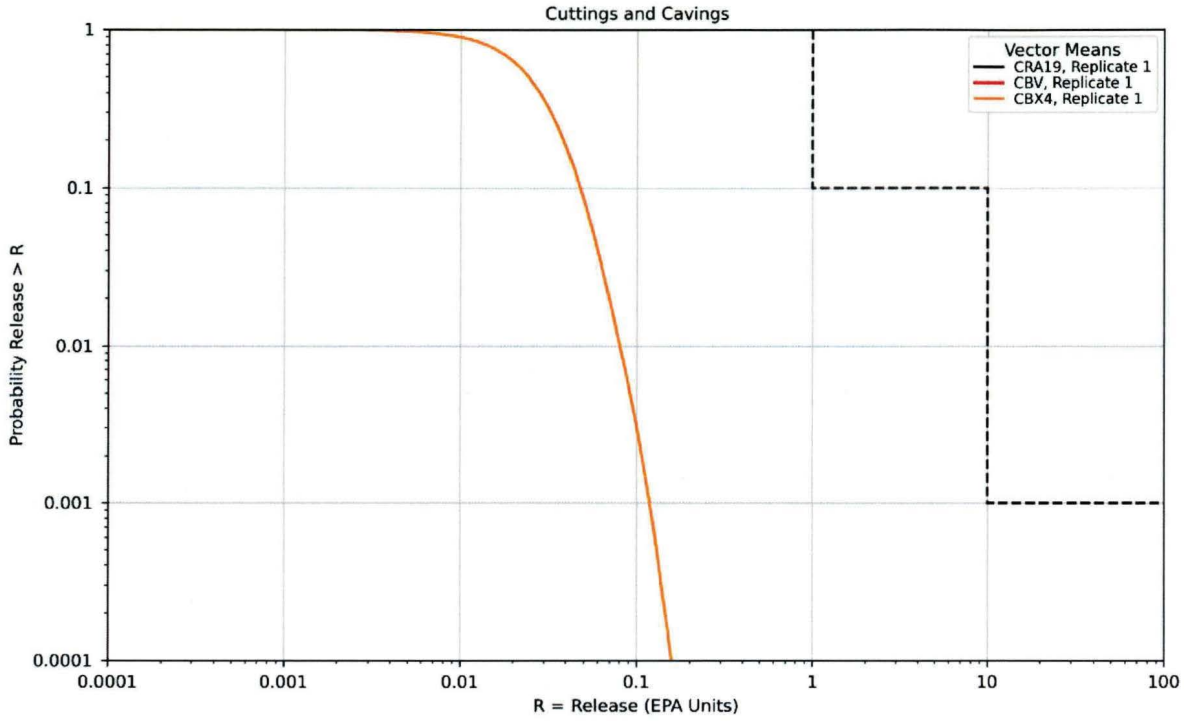


Figure 7: Cuttings and cavings releases

5.0 ANALYSIS OF RESULTS

Conditions in the Castile brine reservoir affect releases only in modeling scenarios that include an E1 intrusion. In an E1 intrusion, a borehole passes through an excavated area of the repository and then into a region of pressurized brine in the Castile. The PA BRAGFLO code, which computes two-phase (brine and gas) flow in and around the repository, models six different scenarios (Day, 2019), three of which involve E1 intrusions. The three E1 intrusion scenarios are named S2-BF, S3-BF, and S6-BF. To gain insight into the results of Section 4, one of the three E1 scenarios, S3-BF, is studied in detail below. In the S3-BF scenario an E1 intrusion occurs at time 1,000 years after closure of the repository.

To aid in the analysis, four plots from the S3-BF scenario are included next: Figure 8, showing the cumulative volume of brine traveling up the borehole from the Castile reservoir, measured at the bottom of the lower disturbed rock zone[4]; Figure 9, showing the change in pressure in the Castile brine reservoir; (iii) Figure 10, showing the change in pressure in the waste inside the repository; and Figure 11, showing brine saturation in the waste. The quantities shown are mean values for Replicate 1, Scenario S3-BF, with results from Models CRA19, CBV and CBX4 plotted together[5]. Additionally, while the BRAGFLO code models flow for a period of 10,000 years after closure,

[4] In Figures 1 and 2, at cell x-index 26, y-index 6.

[5] Waste pressure and waste saturation are averaged over the volume labeled Waste Panel in Figures 1 and 2. These averages are volume-weighted averages. Volume Waste Panel, with x-indices 23-29 and y-indices 10-12, is the same in all three models. Castile brine pressure is averaged (also volume-weighted) over the volume labeled Castile Brine Reservoir in Figures 1 and 2. The extent of the brine reservoir was discussed in Section 3.

Information Only

the plots are focused on the time of the intrusion, displaying quantities only in the interval 500-2000 years. The main feature in the plots is a step change in all quantities at the time of the intrusion. All curves also show an abrupt change in slope at time 1200 years. At this time there is a material change in the intruding borehole: concrete borehole plugs are assumed to have failed, and the entire model borehole is assigned the material properties of a silty sand (see, for example, Appendix PA-2019, US DOE (2019)).

Waste brine saturation and waste pressure are two key drivers of releases from the repository. As Figure 11 indicates, mean brine saturation in the waste rises to a similar level, above 80%, in all three models as brine from the Castile floods the repository soon after the E1 intrusion. The mean waste pressure shown in Figure 10, on the other hand, reaches markedly different levels in the three models. The discrepancy is greatest between Models CRA19 and CBV, and least between CRA19 and CBX4, as was the case for releases in Figures 3-6.

As can be seen in Figure 9, the reservoir loses pressure after the intrusion as it discharges brine up the borehole. Comparing Figures 9 and 10, the greater the mean pressure loss in the reservoir, the smaller the mean pressure increase in the repository. Of interest, therefore, is what causes the pressure drop in the brine reservoir to be different in the three models. The following discussion focuses on the Productivity Ratio of the reservoir. The discussion is divided into two comparisons: CBV vs CRA19; and CBX4 vs CRA19.

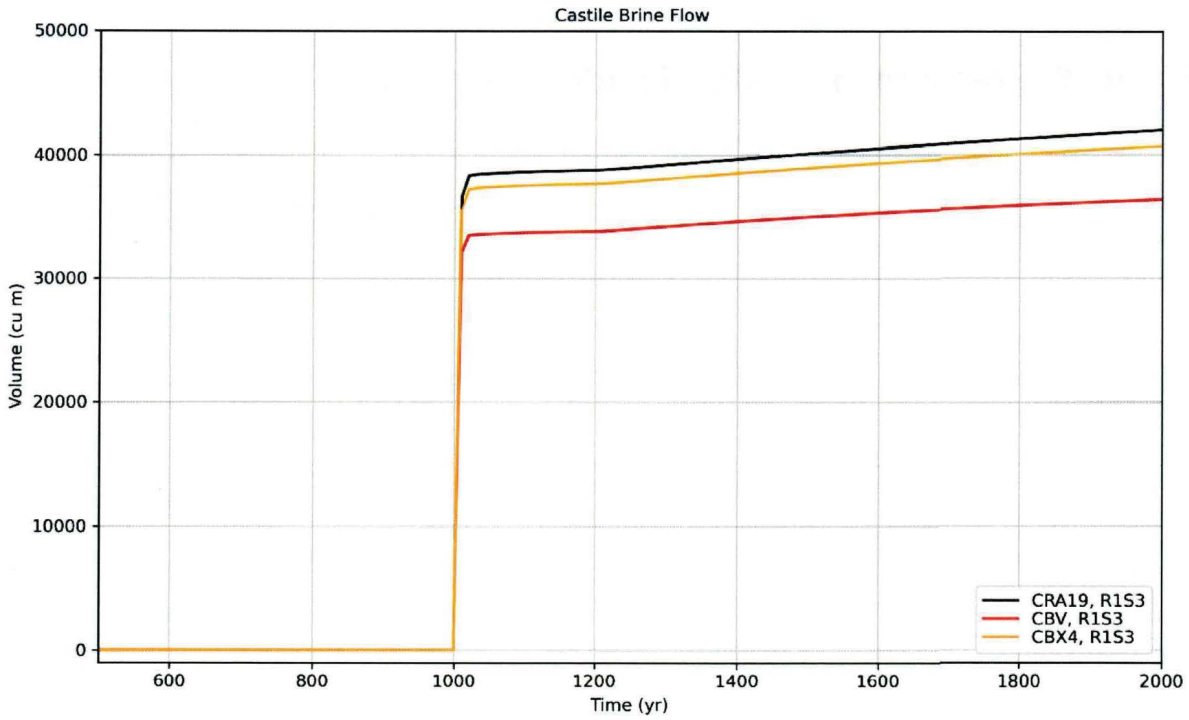


Figure 8: Brine flow up the borehole

Information Only

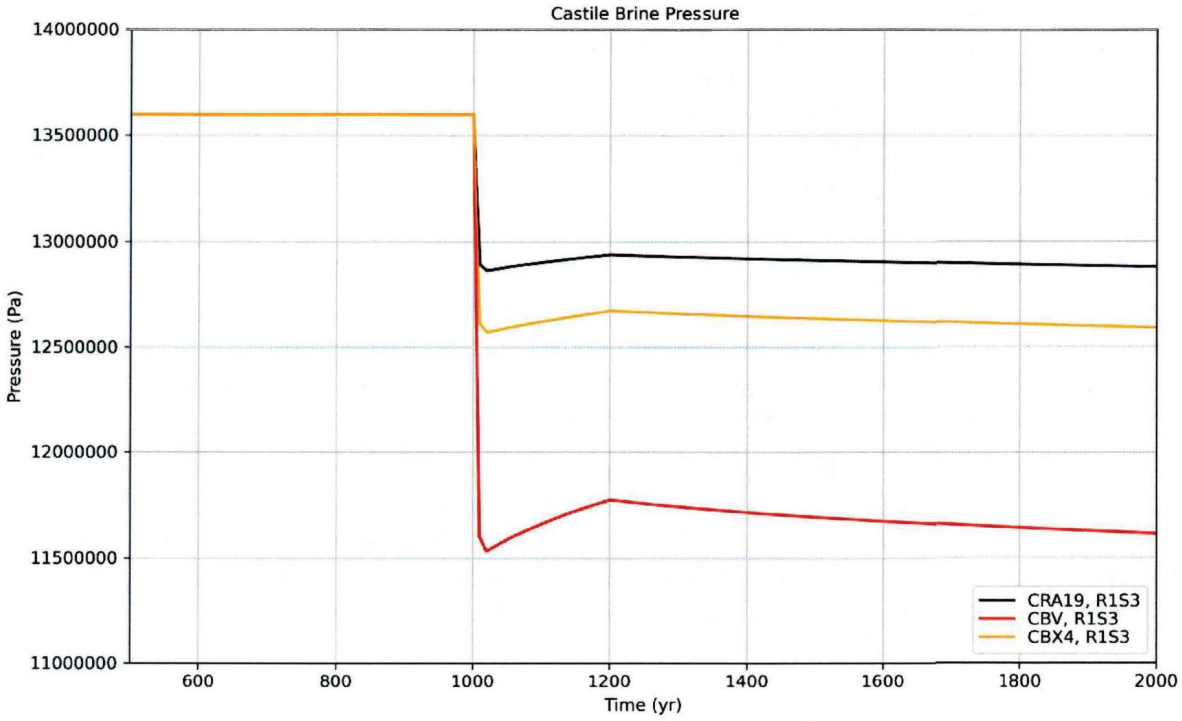


Figure 9: Pressure in the Castile brine reservoir

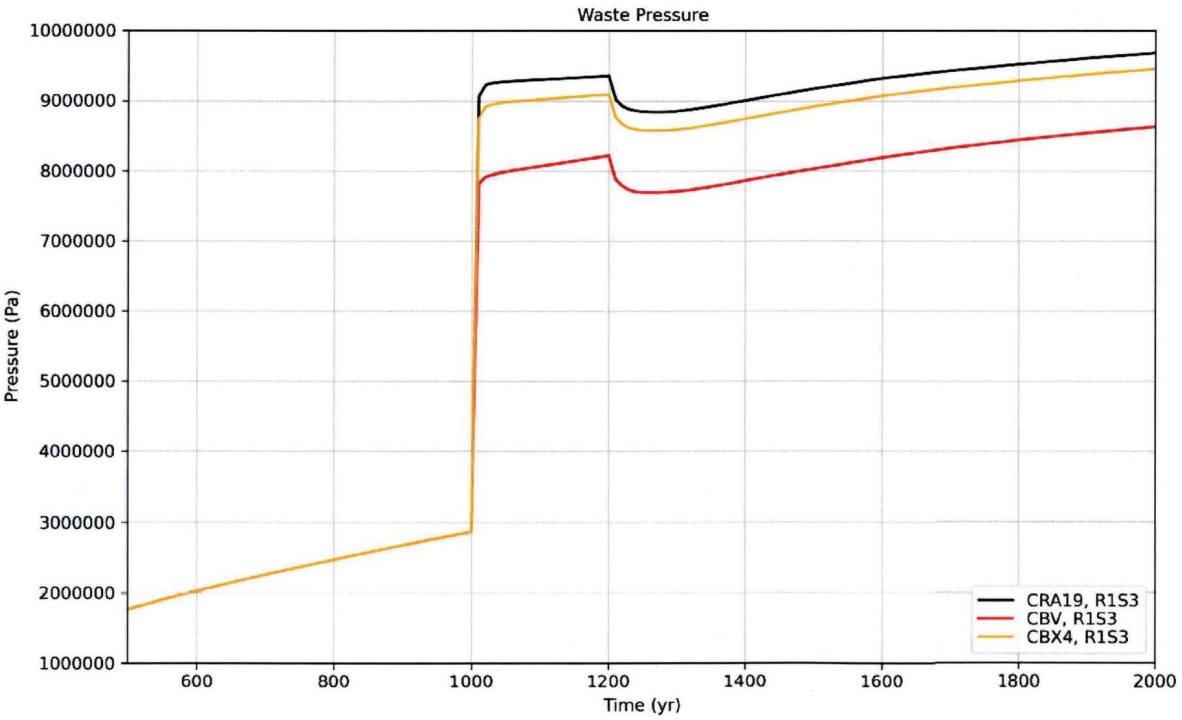


Figure 10: Waste pressure

Information Only

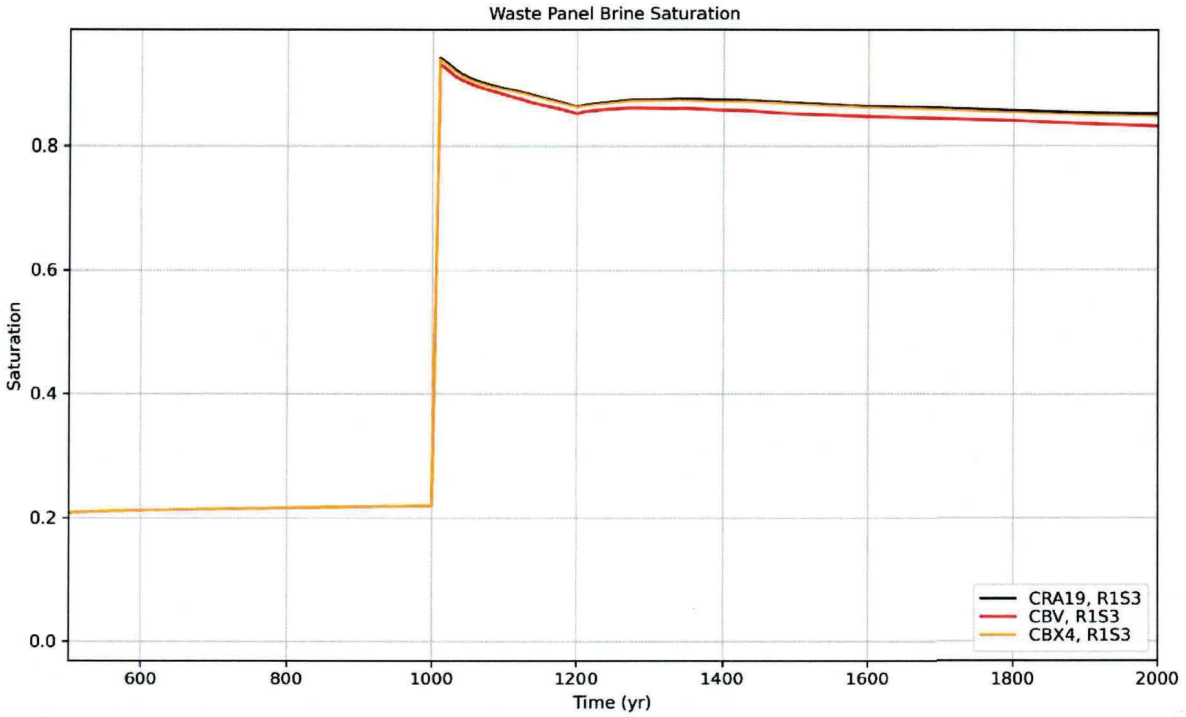


Figure 11: Waste brine saturation

5.1 Brine reservoir pressure: CBV vs CRA19

The Productivity Ratio, equal to dV_ϕ/dP in Eq. 3, can be used to estimate a drop in reservoir pressure dP following a depletion in reservoir volume dV_ϕ. Rewriting Eq. 3 specifically for Models CBV and CRA19, that is, using porosity 0.0087:

$$\frac{dV_\phi}{dP} = c_\phi V_\phi \approx \frac{c_b}{0.0087} V_\phi \quad . \tag{15}$$

For a given value of c_b, the pore volume V_ϕ in Model CBV is a factor of 0.294 times its size in Model CRA19 – roughly speaking, a little less than one third. (The factor turns out to be just the ratio of α values for the two models: see Section 2.) From the left-hand side of Eq. 15, if both models were depleted by the same volume dV_ϕ, then the pressure drop in Model CBV would have to be about 3 times greater than in Model CRA19. The effect can be seen in Figures 8 and 9, though it should be kept in mind that the figures show mean values.

5.2 Brine reservoir pressure: CBX4 vs CRA19

This time the two models have different pore volumes and different pore compressibilities. As was the case above, for a given value of c_b, the pore volume in Model CBX4 is about a third its size in Model CRA19. The pore compressibilities in the two models are, in units Pa^{-1},

Information Only

$$c_\phi = \begin{cases} \frac{c_b}{0.0087} & (CRA19) \\ 1.2407 \times 10^{-8} & (CBX4) \end{cases} \quad (16)$$

As stated in Section 2, the mean value of bulk compressibility is 5.33×10^{-11} [Pa^{-1}], giving 6.13×10^{-9} [Pa^{-1}] for the mean value of pore compressibility in Model CRA19. The pore compressibility of Model CBX4 is thus slightly more than twice the mean pore compressibility of Model CRA19. The combined effects of reducing reservoir volume while increasing reservoir pore compressibility in Model CBX4 can be seen in Figures 8 and 9. From Figure 8, the mean volumes delivered by the reservoir are similar for Models CBX4 and CRA19, while from Figure 9, the mean pressure drop in Model CBX4 is about 3/2 times greater than in Model CRA19.

6.0 SENSITIVITY ANALYSIS

Sensitivity analysis aims to identify those input parameters that have the greatest impact on uncertainty in modeling outcomes. The specific outcomes considered in this section are waste pressure, waste saturation, and brine flow from the Castile reservoir. Of interest is whether these quantities are sensitive to the same, or different, input parameters for Models CRA19, CBV and CBX4; and to what extent, if any, uncertainty in these quantities is affected by differences in the Castile brine reservoir in the three models.

Horsetail plots for Castile brine flow, waste pressure and waste saturation are shown in Figure 12, with results for the three models plotted side by side. Each horsetail plot shows variation over the full 10,000-year modeling period for Replicate 1, Scenario S3-BF. There are 100 curves in each horsetail plot, one for each parameter vector in Replicate 1. (Mean value curves were shown in Figures 8, 10 and 11.) Choosing, for example, waste pressure, corresponding curves in the three models are identical before the intrusion at 1000 years. There is then a step increase in pressure, largest on average in Model CRA19 (Figure 10), at time 1000 years, followed by a rapid divergence of the pressure curves with the change in borehole properties at time 1200 years; pressure evolves similarly after this time in all three models. Horsetails for Models CRA19 and CBX4 are most alike; in comparison, the smaller average step increase in pressure in Model CBV at the time of the intrusion tends to shift its pressure curves down for later times. Significantly, variation across horsetails, that is, uncertainty in outcomes, is very similar for all three models. The horsetails for waste brine saturation and Castile brine flow show less sensitivity to the change in borehole parameters at 1200 years; overall uncertainty appears less for both variables compared to uncertainty in waste pressure; and, as for waste pressure, uncertainty is not significantly different in the three models.

While horsetail plots indicate uncertainty by rendering variability in possible outcomes, they do not reveal which parameters affect the uncertainty. Regression analysis, specifically the PA program STEPWISE (Zeitler, 2019), can provide insight into the importance of individual variables on outcomes. Tables 2-4 show the results of three STEPWISE runs, where the dependent variable was taken to be, in turn, Castile brine flow, waste pressure, and waste brine saturation. For these STEPWISE analyses, the values of the dependent variables at time 10,000 years were input. Looking first at Table 3, the regression for waste pressure is dominated by the parameter

Information Only

BH_SAND:PRMX_LOG with a coefficient of determination, R^2 in the table, of around 0.6 for all three models. BH_SAND:PRMX_LOG is the logarithm of the permeability of the silty-sand that fills the borehole after time 1200 years; its value is described in the database by a uniform probability distribution. An R^2 of 0.6 means this parameter accounts for most of the variability, or uncertainty, in the evolution of waste pressure after the change in borehole properties. (An R^2 of 1.0 would mean this parameter accounted for all of the uncertainty.) The magnitudes of the standardized rank regression coefficients, or SRRCs, in Table 3 further indicate the importance of BH_SAND:PRMX_LOG on waste pressure, while their negative sign means that waste pressure decreases as borehole permeability increases. Note that reservoir bulk compressibility (CASTILER:COMP_RCK) – the parameter determining pore compressibility in Models CRA19 and CBV, and reservoir volume in all three models – does not appear in Table 3.

Looking next at waste brine saturation in Table 4, BH_SAND:PRMX_LOG is again the most important parameter, though less dominant here than it is for waste pressure (compare R^2 and SRRC values). After BH_SAND:PRMX_LOG, the next most important variables influencing waste brine saturation are, in all three models, WAS_AREA:SAT_RGAS and DRZ_1:PRMX_LOG; these parameters describe waste area residual gas saturation and intrinsic permeability in the disturbed rock zone, respectively. Bulk compressibility of the brine reservoir is not detected by STEPWISE as a parameter affecting waste brine saturation.

The situation is somewhat different in Table 2 where, not unexpectedly, STEPWISE finds the ability of the Castile reservoir to deliver brine up the borehole is influenced strongly by reservoir pressure (CASTILER:PRESSURE) in all three models and, via bulk compressibility (CASTILER:COMP_RCK), by pore compressibility in Models CRA19 and CBV. (Recall that Model CBX4 has constant pore compressibility.) For Models CRA19 and CBX4, BH_SAND:PRMX_LOG again features most prominently; in fact, these two models list the same four parameters, in order, as having the greatest influence on brine flow from the reservoir.

To sum up, the different Castile brine reservoir properties in Models CRA19, CBV and CBX4 do not have a significant effect on uncertainty associated with waste pressure, waste saturation, and brine flow from the reservoir. Further, STEPWISE analysis shows uncertainty being influenced by largely the same parameters for all three models – with one exception: brine flow up the borehole in Model CBV is strongly influenced by Castile bulk compressibility.

Information Only

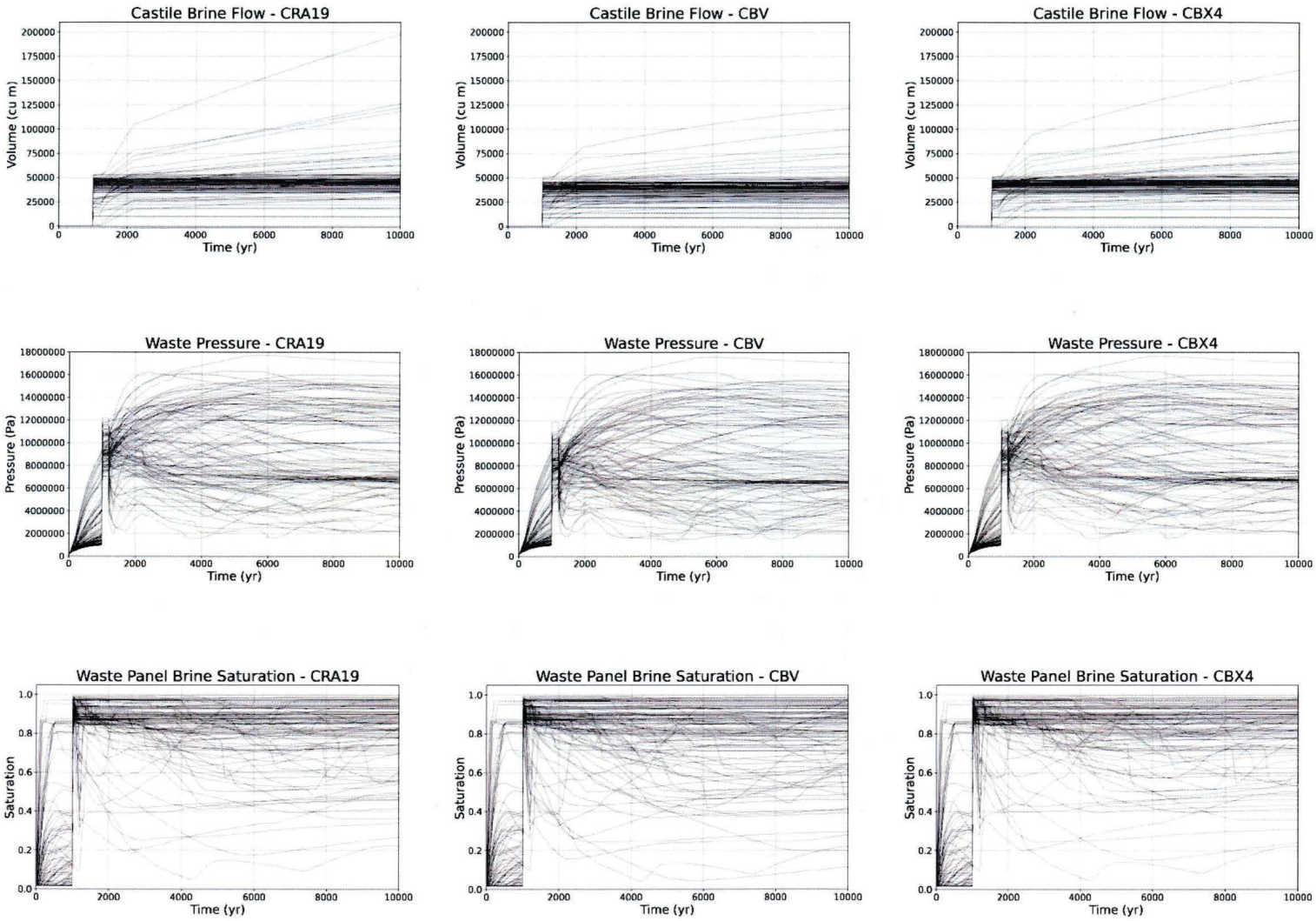


Figure 12: Comparison of brine flow (top), waste pressure (middle), and waste saturation (bottom), for Models CRA19, CBV and CBX4 (Replicate 1, Scenario 3).

Information Only

Table 2: Stepwise ranked regression for brine flow up the borehole

	CRA19			CBV			CBX4		
Step	Variable	R^2	SRRC	Variable	R^2	SRRC	Variable	R^2	SRRC
1	BH_SAND:PRMX_LOG	0.23	0.52	CASTILER:COMP_RCK	0.23	0.49	BH_SAND:PRMX_LOG	0.20	0.48
2	CASTILER:PRESSURE	0.40	0.41	BH_SAND:PRMX_LOG	0.36	0.38	CASTILER:PRESSURE	0.40	0.45
3	S_HALITE:POROSITY	0.46	-0.25	CASTILER:PRESSURE	0.46	0.32	S_HALITE:POROSITY	0.46	-0.25
4	S_MB139:PRMX_LOG	0.50	-0.19	S_HALITE:POROSITY	0.54	-0.28	S_MB139:PRMX_LOG	0.50	-0.19
5	CASTILER:COMP_RCK	0.53	0.17	S_MB139:PRMX_LOG	0.57	-0.19	S_MB139:PORE_DIS	0.52	0.17
6	STEEL:CORRMCO2	0.55	-0.16	DRZ_1:PRMX_LOG	0.60	-0.17	WAS_AREA:HYMAGCON	0.54	-0.15
7	S_MB139:PORE_DIS	0.57	0.15	WAS_AREA:HYMAGCON	0.62	-0.13	STEEL:CORRMCO2	0.57	-0.15
8	WAS_AREA:HYMAGCON	0.59	-0.13						

Table 3: Stepwise ranked regression for waste pressure

	CRA19			CBV			CBX4		
Step	Variable	R^2	SRRC	Variable	R^2	SRRC	Variable	R^2	SRRC
1	BH_SAND:PRMX_LOG	0.60	-0.77	BH_SAND:PRMX_LOG	0.58	-0.75	BH_SAND:PRMX_LOG	0.61	-0.78
2	SHFTU:SAT_RBRN	0.62	-0.16	SHFTU:SAT_RBRN	0.61	-0.16	SHFTU:SAT_RBRN	0.64	-0.15
3	DRZ_1:PRMX_LOG	0.64	-0.14	S_HALITE:COMP_RCK	0.63	-0.15	WAS_AREA:PROBDEG	0.66	0.16
4	WAS_AREA:PROBDEG	0.67	0.16	WAS_AREA:PROBDEG	0.65	0.15	DRZ_1:PRMX_LOG	0.67	-0.12
5	STEEL:CORRMCO2	0.68	-0.13	WAS_AREA:HYMAGCON	0.67	-0.13	STEEL:CORRMCO2	0.69	-0.13
6	WAS_AREA:HYMAGCON	0.70	-0.12	STEEL:CORRMCO2	0.68	-0.12	WAS_AREA:HYMAGCON	0.70	-0.11

Table 4: Stepwise ranked regression for waste brine saturation

	CRA19			CBV			CBX4		
Step	Variable	R^2	SRRC	Variable	R^2	SRRC	Variable	R^2	SRRC
1	BH_SAND:PRMX_LOG	0.30	0.54	BH_SAND:PRMX_LOG	0.38	0.58	BH_SAND:PRMX_LOG	0.32	0.56
2	WAS_AREA:SAT_RGAS	0.44	-0.37	WAS_AREA:SAT_RGAS	0.50	-0.36	WAS_AREA:SAT_RGAS	0.46	-0.37
3	DRZ_1:PRMX_LOG	0.55	0.33	DRZ_1:PRMX_LOG	0.61	0.33	DRZ_1:PRMX_LOG	0.57	0.33
4	GLOBAL:GDEPFAC	0.58	-0.16	DRZ_PCS:PRMX_LOG	0.64	0.14	(Composite):OXSTAT	0.59	-0.14
5	DRZ_PCS:PRMX_LOG	0.61	0.15	WAS_AREA:SAT_RBRN	0.66	-0.13	DRZ_PCS:PRMX_LOG	0.62	0.15
6	WAS_AREA:SAT_RBRN	0.63	-0.13	GLOBAL:GDEPFAC	0.67	-0.13	GLOBAL:GDEPFAC	0.64	-0.15
7	(Composite):OXSTAT	0.65	-0.14	GLOBAL:OXSTAT	0.69	-0.12	WAS_AREA:SAT_RBRN	0.66	-0.13
8	SHFTU:SAT_RGAS	0.66	-0.13	SHFTU:SAT_RBRN	0.70	0.12			
9	WAS_AREA:BIOGENFC	0.68	-0.13						

Information Only

7.0 IMPLEMENTATION

This section describes those changes necessary to implement Models CBV and CBX4, starting from Model CRA19. The changes are made to PA input files. No changes are required to database (PAPDB) parameters. A final sub-section notes execution on the Linux cluster at WIPP.

7.1 Model CBV

Model CBV differs from Model CRA19 only in the porosity of the Castile brine reservoir. The change is effected through the constant, called α above, relating Castile reservoir porosity and bulk compressibility. The constant is set in the file input to the first instance of ALGEBRACDB in the BRAGFLO computational sequence of PA. Two changes were also made to the file input to the second instance of ALGEBRACDB in order (i) to calculate the volume of brine flowing up the borehole from the Castile (Figure 8); and (ii) to calculate the Castile brine reservoir pressure (Figure 9). In detail these changes are:

1. alg1_bf_xxx.inp: Element Block 11, set POROSITY = CMP_RCK / 3.6915E−10.
2. alg2_bf_xxx.inp: Integrate flow up the borehole at base of lower disturbed rock zone.
3. alg2_bf_xxx.inp: Compute volume-averaged Castile brine reservoir pressure.

Here, xxx denotes the analysis name and Element Block 11 in item 1 identifies the block of grid elements (cells) assigned to the Castile brine.

7.2 Model CBX4

Model CBX4 assigns additional grid cells to the Castile brine reservoir, as well as changing its porosity. Adding cells to the brine reservoir changes Castile grid indices in the input to GENMESH, as well as changing element numbers in several other input files (items 4, 5 and 8-10 below). As was the case for Model CBV, a porosity change is brought about by changing the constant relating porosity to bulk compressibility. In addition, Model CBX4 has pore compressibility set equal to bulk compressibility divided by porosity. Brine flow up the borehole and Castile brine reservoir pressure are calculated as they are for Model CBV. The full list of changes is:

1. gm_bf_xxx.inp: change Castile and Castiler grid indices.
2. alg1_bf_xxx.inp: Element Block 11, set POROSITY = CMP_RCK / 1.2407E−8.
3. alg1_bf_xxx.inp: Element Block 11, set POR_CMP = COMP_RCK/POROSITY after POROSITY is determined from bulk compressibility (item 1 above).
4. alg1_bf_xxx.inp: change element numbers when setting pressure in Castile, Rustler, Dewey Lake, Santa Rosa, Culebra, and Magenta.
5. alg1_bf_xxx.inp: change element numbers when accounting for dip in Castile and regions above the Salado.
6. alg2_bf_xxx.inp: Integrate flow up the borehole at base of lower disturbed rock zone.
7. alg2_bf_xxx.inp: Compute volume-averaged Castile brine reservoir pressure.
8. cusp_xxx.inp: change element number of borehole Castile intersect.
9. alg_nut_iso.xxx.inp: change element number of borehole Culebra intersect.
10. alg_nut_scn:xxx.inp: change element number of borehole Culebra intersect.

Information Only

7.3 Execution on Linux cluster

PAs for Models CBV and CBX4 were run on the Linux cluster at WIPP and not on the Solaris cluster as described by King et al. (2022) in the original analysis plan. As reported by Long and King (2022), PA results generated on the Linux cluster are nearly identical to PA results generated on the Solaris cluster for mean values, and there are few differences at vector level. Use of the Linux cluster instead of the Solaris cluster is not expected to have impacted the results presented here.

8.0 SUMMARY AND RECOMMENDATION

A Castile brine reservoir maximum volume estimate determined by Gross and Gjerapic (2022) was implemented and tested in two PA models. PA results for the two models were compared to results from CRA-2019. The model from CRA-2019 was named Model CRA19 here.

The first model tested, called CBV, differed from Model CRA19 only in the porosity of cells assigned to represent the brine reservoir. Model CBV was useful in demonstrating the effect on releases of making this change alone. In CRA-2019, and in previous CRAs dating back to 2004, the porosity in the brine reservoir was set artificially high, in the range 18-92%, in order to accommodate a desired range of reservoir volume. In Model CBV the porosity was reduced by a factor of about a third, though at 5-27% these values are still considered high for the fractured anhydrite at WIPP. The effect of reducing porosity, and thus pore volume, was to reduce the productivity of the brine reservoir. As a result, there was a greater loss of pressure in the reservoir following an intrusion, a smaller volume of brine was delivered to the repository, pressure in the waste did not rise to as high a level as it did in CRA-2019, and direct brine releases of waste were significantly less than in CRA-2019.

The second model tested, called CBX4, extended the brine reservoir laterally by about 800 m at each end. This increased the volume of model grid cells assigned to the reservoir by a factor of more than thirty, enabling Gross and Gjerapic's maximum volume estimate to be implemented with porosity in the range 0.1-0.8%. The new range of porosity was used to set pore compressibility in Model CBX4, on average causing its value to double. Reducing reservoir volume while increasing pore compressibility meant that reservoir productivity was not greatly affected. As a result, Model CBX4 waste pressure and waste releases following an intrusion were not appreciably different to their levels in CRA-2019.

Differences in the brine reservoir implementations had little effect on uncertainties associated with waste pressure, waste brine saturation, and brine flow up the borehole into the repository. Similarly, parameters that most strongly influence uncertainty in these quantities were found to be the same in all three models, with one exception: reservoir bulk compressibility features more prominently in controlling brine flow up the borehole in Model CBV than it does in Models CBX4 and CRA19.

Reservoir porosity is the most notable difference between Models CRA19, CBV and CBX4. Only the Model CBX4 range of porosities can be considered physically realistic. Comparing favorably with historical estimates, the CBX4 porosities enabled a treatment of reservoir pore compressibility consistent with other materials in PA. Further, these advantages combined to give a mean Productivity Ratio of 0.04 for Model CBX4, which is precisely the value obtained from well WIPP-12 data. For these reasons, for its relative ease of implementation, and because it

Information Only

produces outcomes and uncertainties similar to those observed in CRA-2019, it is recommended that the Castile brine reservoir described in Model CBX4 be used for future PA calculations.

9.0 REFERENCES

Beauheim, R. 1996. Memorandum to Les Shephard. Subject: Treatment of brine reservoirs in CCA. Sandia National Laboratories, Albuquerque, NM.

Day, B. 2019. Analysis Package for Salado Flow in the 2019 Compliance Recertification Application Performance Assessment (CRA-2019 PA). Carlsbad, NM: Sandia National Laboratories. ERMS 571368.

Gross, M. B., and G. Gjerapic. 2022. Analysis to bound reservoir volumes for WIPP Performance Assessment (Rev. 02). Nuclear Waste Partnership, Carlsbad, NM.

Helton, J. C., J. E. Bean, J. W. Berglund, F. J. Davis, K. Economy, J. W. Garner, J. D. Johnson, R. J. MacKinnon, J. Miller, D. G. O'Brien, J. L. Ramsey, J. D. Schreiber, A. Shinta, L. N. Smith, D. M. Stoelzel, C. Stockman, and P. Vaughn. 1998. Uncertainty and sensitivity analysis results obtained in the 1996 Performance Assessment for the Waste Isolation Pilot Plant. Sandia National Laboratories, Albuquerque, NM. SAND98-0365. ERMS 252619.

King, S., C. Hansen, and J. Bethune. 2022. Analysis plan for modeling the pressurized Castile brine reservoir. Sandia National Laboratories, Carlsbad, NM. ERMS 576846.

Long, J., and S. King. 2022. Summary report on the migration of the WIPP PA codes from Solaris to Linux (AP-184, Rev. 0). Sandia National Laboratories, Carlsbad, NM. ERMS 577606.

Popielak, R. S., R. L. Beauheim, S. R. Black, W. E. Coons, C. T. Ellingson, and R. L. Olsen. 1983. Brine reservoirs in the Castile formation, Waste Isolation Pilot Plant, Southeastern New Mexico. U. S. Department of Energy, Carlsbad, NM. TME 3153.

Stein, J. S. 2003. Memorandum to David Kessel. Subject: Correlation between bulk compressibility and porosity in the Castile brine pocket as modeled in BRAGFLO. Sandia National Laboratories, Carlsbad, NM. ERMS 527293.

U.S. Department of Energy (DOE). 2019. Title 40 CFR Part 191 Compliance Recertification Application for the Waste Isolation Pilot Plant. Carlsbad, NM: U.S. Department of Energy, Carlsbad Field Office. DOE/WIPP 2019-3609.

U.S. Environmental Protection Agency 1997. Technical support document for Section 194.23, Sensitivity analysis report. Docket A-93-02, Item V-B-13.

U.S. Environmental Protection Agency 1998. Technical support document for Section 194.23, Parameter justification report. Docket A-93-02, Item V-B-14.

Zeitler, T. 2019. Analysis package for the sensitivity of releases to input parameters in the 2019 Compliance Recertification Application Performance Assessment (CRA-2019 PA). Sandia National Laboratories, NM. ERMS 571374.

Information Only

Appendix A: Mean values in Table 1

Bulk compressibility c_b is a sampled parameter in PA described by a triangular probability distribution (that is, a triangular probability density function) like the one sketched in Figure 13. From Eq. 1, the triangular distribution for c_b has $x_{min} = 2.0\times10^{-11}$, $x_{max} = 1.0\times10^{-10}$, and, as mentioned in Section 2, $x_{mode} = 4.0\times10^{-11}$ (all with units Pa^{-1}). Note that for c_b's distribution, $x_{mode} = (3x_{min}+x_{max})/4$.

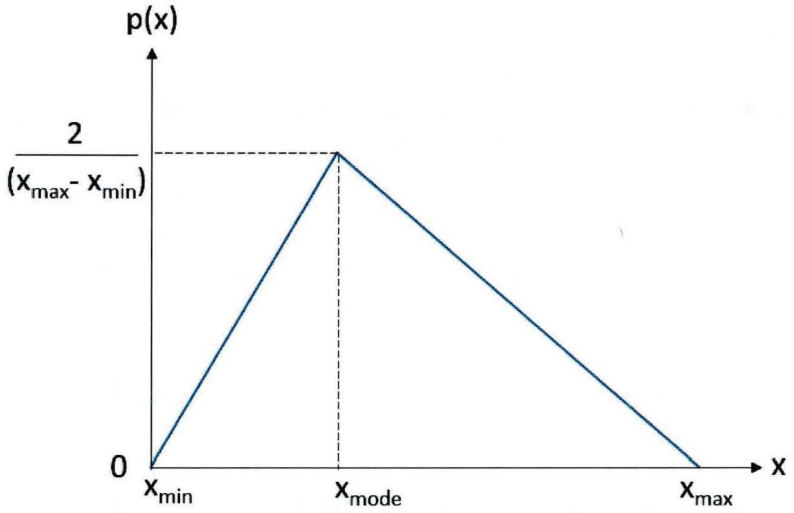


Figure 13: Triangular probability distribution

To obtain the mean values given in Table 1 it is first necessary to obtain the mean values of c_b and c_b^2. The mean, or expected value, of c_b can be obtained by integration:

$$E(c_b) = \int_{2\times10^{-11}}^{1\times10^{-10}} p(c_b)\, c_b\, dc_b = 5.333 \times 10^{-11} \quad .$$

Here, $p(c_b)$ is the probability distribution for c_b. The integral is easily evaluated by splitting the range of integration into two parts corresponding to the slanted sides of c_b's triangular distribution. Likewise, it is straightforward to determine the expected value of c_b^2:

$$E(c_b^2) = \int_{2\times10^{-11}}^{1\times10^{-10}} p(c_b)\, c_b^2\, dc_b = 31.333 \times 10^{-22} \quad .$$

The mean values for reservoir porosity ϕ, pore volume V_ϕ, and reservoir pore compressibility c_ϕ in Table 1 are then obtained as

Information Only

$$E(\phi) = E\left(\frac{c_b}{\alpha}\right) = \frac{1}{\alpha} E(c_b) \ ,$$

$$E(V_\phi) = E(\phi V) = \frac{V}{\alpha} E(c_b) \ ,$$

$$E(c_\phi) = \frac{1}{0.0087} E(c_b) \ , \qquad \textit{Models CRA19 and CBV,}$$

$$E(c_\phi) = E\left(\frac{c_b}{\phi}\right) = \alpha \ , \qquad \textit{Model CBX4} \ .$$

In these equations, V is grid volume and α is the constant introduced in Eq. 5. The mean values of Productivity Ratio PR given in Table 1 are obtained from

$$E(PR) = E(c_\phi V_\phi) = E\left(\frac{c_b}{0.0087}\phi V\right) = \frac{V}{0.0087\,\alpha} E(c_b^2) \ , \ \textit{Models CRA19 and CBV} \ ,$$

and

$$E(PR) = E(c_\phi V_\phi) = E\left(\frac{c_b}{\phi}\phi V\right) = V\,E(c_b) \ , \qquad \textit{Model CBX4} \ .$$

Finally, note the variables in Table 1 that have probability distributions geometrically similar to the triangular distribution of bulk compressibility: porosity ϕ, pore volume V_ϕ, pore compressibility c_ϕ in Models CRA19 and CBV, and PR in Model CBX4. As an example, the distribution for reservoir porosity in Model CRA19 would be Figure 13 with x_{min} and x_{max} from Eq. 9, and $x_{mode} = (3x_{min}+x_{max})/4$, as in the distribution for c_b. Two distributions not mentioned, namely the distributions for PR in Models CRA19 and CBV, are geometrically similar to the distribution of c_b^2 rather than the distribution of c_b.

Information Only